Potential of Spheroids in a Homogeneous Magnetic Field in Cartesian Coordinates

Markus Kraiger* and Bernhard Schnizer†

*Institute for Radiopharmacy - PET Center, Helmholtz-Zentrum Dresden - Rossendorf e.V., Bautzner Landstr. 400, D-01328 Dresden - Schönfeld/Schullwitz, Germany. Email: m.kraiger@hzdr.de

† Institute for Theoretical Physics - Computational Physics, Technische Universität Graz, Petersg. 16, A-8010 Graz, Austria

E-mail: schnizer@itp.tu-graz.ac.at

Abstract—**The potential and the field of a prolate or an oblate magnetic spheroid in a static homogeneous field are computed and expressed in Cartesian coordinates. The directions of both the primary magnetic field and of the symmetry axis are completely arbitrary. These expressions are used to investigate trabecular structures built from spheroids having different symmetry axes and positions for Magnetic Resonance (MR-) Osteodensitometry.**

Index Terms—**Prolate or oblate spheroid in homogeneous field, building flexible models for magnetic resonance imaging or spectroscopy.**

I. INTRODUCTION

In gerneral, the potential of a magnetic spheroid in a given external magnetic field is derived in spheroidal coordinates, whose symmetry axis is the z-axis. Models of biological tissues, as e.g. trabecular bones, are arrays of such spheroids with symmetry axes having various directions. Having such applications in mind, we derived potential and field expressions for prolate and oblate spheroids in a homogeneous field. These expressions depend on Cartesian coordinates for arbitrary directions of both the field and the symmetry axes.

II. METHOD OF SOLUTION

A spheroid (permeability $\mu_i = \mu_0(1 + \chi_i)$; semi-axes a, a, c) is in a medium (permeability $\mu_e = \mu_0(1 + \chi_e)$) and a static homogeneous field $\mathbf{H}_0 = (H_{0x}, H_{0y}, H_{0z}) = H_0(\sin\beta\ \cos\alpha, \sin\beta\ \sin\alpha, \cos\beta)$ of arbitrary direction. At first the problem of a prolate spheroid is solved in prolate spheroidal coordinates ([1], Fig.1.06)

$$\begin{aligned} x + iy &= e_p\ \sinh\eta\ \sin\theta\ e^{i\psi} \\ z &= e_p\ \cosh\eta\ \cos\theta \end{aligned} \quad (1)$$

or in the corresponding oblate spheroidal coordinates ([1], Fig.1.07)

$$\begin{aligned} x + iy &= e_o\ \cosh\eta\ \sin\theta\ e^{i\psi} \\ z &= e_o\ \sinh\eta\ \cos\theta. \end{aligned} \quad (2)$$

for an oblate spheroid as shown e.g. in [2] to [4]. The particular solutions of the potential equation are obtained by separation giving Legendre functions and polynomials of $\cosh\eta$, $i\sinh\eta$ respectively multiplied by Legendre polynomials of $\cos\theta$ and by trigonometric functions of ψ. A solution of this problem is found by the usual method, namely by expanding the potential in the interior and in the exterior of the spheroid w.r.t. the particular solutions fulfilling the appropriate boundary conditions: i) the total potential must be finite at $\eta = 0$; ii) the total potential must agree with that of the primary field (5) at $\eta = \infty$. The expansion coefficients are determined by the continuity conditions that the total potential must be continuous $\Phi_0 + \Phi_e^\sigma = \Phi_0 + \Phi_i^\sigma$ and the corresponding normal component of the magnetic induction must be continuous at the interface of the two media ((7) with $\mathbf{n} = \mathbf{e}_z$). The solutions contain only Legendre funtions and polynomials of order 1

since the inhomogeneity (5) is of that order. Thereafter the Legendre functions and polynomials may be replaced with elementary functions of η and θ. These may be in turn expressed by functions of Cartesian coordinates by use of (1), (2) respectively and by $\cosh\eta = u_p(\mathbf{r}, \mathbf{e}_z)/\sqrt{2}$, $\sinh\eta = u_o(\mathbf{r}, \mathbf{e}_z)/\sqrt{2}$, eq.(24) respectively. The expansion coefficients $L_0^\sigma, L_1^\sigma, M_0^\sigma, M_1^\sigma$ obtained from matching the two pieces of the potential at the interface are first expressed in Legendre functions and polynomials of argument η_p, η_o respectively:

$$\begin{aligned} \eta_p &= \text{Arcoth}(c_p/a_p) &\quad (3) \\ \eta_o &= \text{Artanh}(c_o/a_o). &\quad (4) \end{aligned}$$

The coefficients are also reexpressed in elementary functions of these geometrical parameters and by the magnetic susceptibilities χ_e, χ_i to give eqs.(8) to (11), (13) to (16) respectively. In the last step the potential in both domains is transformed to an arbitrary direction $\mathbf{n}$ of the spheroidal symmetry axis. All vectors in the potential are decomposed into vectors parallel to or perpendicular to the z-axis. Finally all vectors $\mathbf{e}_z$ occuring in these expressions are replaced by $\mathbf{n}$.

This description is rather concise; full details may be found in the papers [3] and [4] and in the notebooks at the website quoted. But the next paragraph gives a complete listing of all formulas needed for the applications.

III. RESULTS

The primary field is homogeneous with the potential

$$\Phi_0(x, y, z) = -(H_{0x}\ x + H_{0y}\ y + H_{0z}\ z). \quad (5)$$

A. The potentials of the reaction fields

The presence of a spheroid induces a reaction field with potential ($\mathbf{r} = (x_\beta)$) :

$$\Phi_k^\sigma(x, y, z) = \sum_{\alpha,\beta=1}^{3} H_{0\alpha} t_{\alpha\beta}^{\sigma,k} x_\beta = \mathbf{H}_0 \cdot \mathbf{T}^{\sigma,k} \cdot \mathbf{r} \quad (6)$$

with $\sigma = p$ (= prolate) or $= o$ (= oblate) and k = e (= external) or i (= internal) to the ellipsoid

$$\mathcal{E}_\sigma := \frac{r^2 - (\mathbf{n} \cdot \mathbf{r})^2}{a_\sigma^2} + \frac{(\mathbf{n} \cdot \mathbf{r})^2}{c_\sigma^2} = 1. \quad (7)$$

For a prolate spheroid, $a_p < c_p$, the excentricity is $e_p = \sqrt{c_p^2 - a_p^2}$; for an oblate one, $c_o < a_o$, and the excentricity is $e_o = \sqrt{a_o^2 - c_o^2}$.

The coefficients $L_0^\sigma, L_1^\sigma, M_0^\sigma, M_1^\sigma$ depend only on the geometric shape of the spheroids, i.e. on the semi-axes a_σ, c_σ, and on the magnetic susceptibilites χ_1, χ_2. The former dependence is through the functions η_p, η_o (eqs.(3), (4)) respectively of the quasi-radial prolate or oblate elliptical coordinates corresponding to the interface $\mathcal{E}_\sigma = 1$. But all expressions depending on η_p, η_o may be replaced by functions of the $a_\sigma, c_\sigma, e_\sigma$:

$$L_0^p = [(\chi_1 - \chi_2)c_p/e_p]/D_0^p \tag{8}$$
$$D_0^p = 1 + \chi_2 - (1 + \chi_1)c_p^2/a_p^2 + (\chi_1 - \chi_2)\, d_p c_p/a_p$$
$$L_1^p = [\chi_1 - \chi_2]/D_1^p \tag{9}$$
$$D_1^p = (2 + \chi_1 + \chi_2) - (\chi_1 - \chi_2)\, a_p^2/e_p^2\, (1 - d_p c_p/e_p)$$
$$M_0^p = -(1 + \chi_1)/D_2^p \tag{10}$$
$$D_2^p = 1 + \chi_1 + (\chi_1 - \chi_2)\, a_p^2/e_p^2\, (1 - d_p c_p/e_p)$$
$$M_1^p = [-2(1 + \chi_1)]/D_1^p \tag{11}$$
$$d_p = \operatorname{Arcoth}(c_p/e_p) \tag{12}$$

$$L_0^o = [(\chi_1 - \chi_2)c_o/e_o]/D_0^o \tag{13}$$
$$D_0^o = (1 + \chi_2) - (1 + \chi_1)\, c_o^2/a_o^2 + (\chi_1 - \chi_2)\, d_o c_o/e_o$$
$$L_1^o = -[(\chi_1 - \chi_2)\, a_o^2 c_o/e_o^3]/D_1^o \tag{14}$$
$$D_1^o = (2 + \chi_1 + \chi_2) + (\chi_1 - \chi_2)\, a_o^2/e_o^2\, (1 - d_o c_o/e_o)$$
$$M_0^o = [(1 + \chi_1)\, e_o^2/a_o^2]/D_0^o \tag{15}$$
$$M_1^o = [2(1 + \chi_1)]/D_1^o \tag{16}$$
$$d_o = \operatorname{arccot}(c_o/e_o). \tag{17}$$

In the exterior, $\mathcal{E}_\sigma \geq 1$ the tensor $\mathbf{T}^{e,\sigma} = (T_{\alpha\beta}^{e,\sigma})$ is:

$$T_{\alpha\beta}^{e,\sigma} = \delta_{\alpha\beta}\, L_1^\sigma\, (f_1^\sigma - f_2^\sigma) + n_\alpha n_\beta [L_0^\sigma\, (f_1^\sigma - f_3^\sigma) - L_1^\sigma\, (f_1^\sigma - f_2^\sigma)] \tag{18}$$

In the interior, $\mathcal{E}_\sigma \leq 1$, the field is homogeneous:

$$T_{\alpha\beta}^{i,\sigma} = \delta_{\alpha\beta}\, (1 \pm M_1^\sigma) \pm n_\alpha n_\beta\, (M_0^\sigma - M_1^\sigma). \tag{19}$$

Above and below the upper (lower) signs apply for $\sigma = p$ (o).

$$f_1^p = \operatorname{Arcoth}\big(u_p(\mathbf{n}, \mathbf{r})/\sqrt{2}\big) \tag{20}$$
$$f_1^o = \operatorname{arccot}\big(u_o(\mathbf{n}, \mathbf{r})/\sqrt{2}\big) \tag{21}$$
$$f_2^\sigma = \sqrt{2}\, u_\sigma(\mathbf{n}, \mathbf{r})/[(u_\sigma(\mathbf{n}, \mathbf{r}))^2 \mp 2] \tag{22}$$
$$f_3^\sigma = \sqrt{2}/u_\sigma(\mathbf{n}, \mathbf{r}) \tag{23}$$
$$u_{p,o}(\mathbf{n}, \mathbf{r}) = \sqrt{\pm 1 + r^2/e_{p,o}^2 + w_{p,o}(\mathbf{n}, \mathbf{r})} \tag{24}$$
$$w_{p,o}(\mathbf{n}, \mathbf{r}) = \sqrt{\big(\pm 1 + r^2/e_{p,o}^2\big)^2 \mp 4(\mathbf{n} \cdot \mathbf{r})^2/e_{p,o}^2} \tag{25}$$

B. The magnetic reaction fields

For the evaluation of the impact of the inhomogeneous field distribution on the MR resonance signals the magnetic reaction fields are needed. The tensors $\mathbf{K}^{\sigma,k} = (K_{\alpha\beta}^{\sigma,k})$ transform the primary field $\mathbf{H}_0 = (H_{0\beta})$ into the reaction fields $\mathbf{H}_k^\sigma = (H_\alpha^{\sigma,k})$:

$$H_\alpha^{\sigma,k}(x, y, z) = \sum_{\beta=1}^{3} K_{\alpha\beta}^{\sigma,k}\, H_{0\beta}, \quad \sigma = p, o; k = e, i. \tag{26}$$

The tensors are found by computing the gradients of the reaction potentials. This requires also the gradients of the functions f_n^σ. Which are evaluated by symbolic computation [4] using *Mathematica*. Since the resulting expressions consist again of polynomials and the square roots already occuring in the exterior potentials it is possible to find simpler expressions. These are again checked against the original gradients by symbolic computation [4]. All gradients are proportional to the vectors $\mathbf{r}^p (= x_\alpha^p), \mathbf{r}^o (= x_\alpha^o)$ respectively:

$$\mathbf{r}^{p,o} := \frac{\sqrt{2}}{e_{p,o}^2}\left(\mathbf{r} \mp 2\mathbf{n}\, \frac{(\mathbf{n} \cdot \mathbf{r})}{[u_{p,o}(\mathbf{r}, \mathbf{n})]^2}\right). \tag{27}$$

The expressions for the reaction tensors of prolate or oblate spheroids with symmetry axis $\mathbf{n}$ in an external homogeneous magnetic field $\mathbf{H}_0$ are then in the exterior:

$$\mathcal{E}_\sigma \geq 1:$$
$$K_{\alpha\beta}^{\sigma,e}(x, y, z) = \tag{28}$$
$$- \delta_{\alpha\beta}\, L_1^\sigma\, (f_1^\sigma - f_2^\sigma) -$$
$$- n_\alpha n_\beta\, [L_0^\sigma\, (f_1^\sigma - f_3^\sigma) - L_1^\sigma\, (f_1^\sigma - f_2^\sigma)]$$
$$\mp x_\alpha^\sigma\, x_\beta\, L_1^\sigma\, \frac{u_\sigma(\mathbf{r}, \mathbf{n})}{w_\sigma(\mathbf{r}, \mathbf{n})}\, \frac{4}{[(u_\sigma(\mathbf{r}, \mathbf{n}))^2 \mp 2]^2}$$
$$- x_\alpha^\sigma\, n_\beta\, (\mathbf{r} \cdot \mathbf{n})\, L_0^\sigma\, \frac{2}{[2 \mp (u_\sigma(\mathbf{r}, \mathbf{n}))^2]u_\sigma(\mathbf{r}, \mathbf{n})\, w_\sigma(\mathbf{r}, \mathbf{n})}$$
$$\pm x_\alpha^\sigma\, n_\beta\, (\mathbf{r} \cdot \mathbf{n})\, L_1^\sigma\, \frac{4\, u_\sigma(\mathbf{r}, \mathbf{n})}{w_\sigma(\mathbf{r}, \mathbf{n})\, [(u_\sigma(\mathbf{r}, \mathbf{n}))^2 \mp 2]^2}.$$

The upper, lower signs respectively apply to prolate ($\sigma = p$), oblate ($\sigma = o$) spheroids respectively. The fields in the interior are homogeneous, but are not parallel to the primary field, in general:

$$\mathcal{E}_\sigma \leq 1:$$
$$K_{\alpha,\beta}^{\sigma,i}(x, y, z) = \tag{29}$$
$$- \delta_{\alpha\beta}\, (M_1^\sigma \pm 1) - n_\alpha n_\beta\, (M_0^\sigma - M_1^\sigma).$$

The theory above has been derived under the assumption that the spheroid is centred at the origin. If the centre is at the point $\mathbf{r}_0$ then $\mathbf{r}$ must be replaced by $\mathbf{r} - \mathbf{r}_0$ in all formulas.

IV. APPLICATION: MODELLING TRABECULAR BONE

Applications presuppose that the magnetic susceptibilities of the medium and of the spheroids are small. So the total magnetic induction at the location of a proton spin is approximated by that of the primary field and those of the reaction fields of all spheroids. One application from the area of MR-Osteodensitometry is given: modelling of micro cracks in bone structures as examples of trabecular rarefaction.

A. Introduction: MR-Osteodensitometry

Generally, in magnetic resonance experiments disturbances of the homogeneous main magnetic field have an essential impact on the formation of the resonance signal. Especially in MR-Osteodensitometry information about the status of cancellous bone can be gained based on susceptibility effects between the mineralized bone and bone marrow [5]. In the presence of trabeculae the relaxation properties of bone marrow are changed due to the inhomogeneity of the magnetic field, induced by the discontinuities of the magnetic susceptibility across the surface of the bone [6]. In several studies direct relations between the effective transversal relaxation time with bone mineral density (BMD) [7], [8], [9] and with mechanical competence of trabecular bone [10], [11], [12] were reported.

The resonance signal decay in a gradientecho MR experiment obeys, in case of these inhomogeneities being of Lorentzian characteristics, the following empirical expression:

$$S(T_E) \propto e^{-R_2^* T_E} \quad \text{with} \quad R_2^* = 1/T_2 + R_2', \tag{30}$$

with T_2 giving the intrinsic transversal relaxation time and T_E the echo time. The quantity $R_2' = 1/T_2'$ accounts for

the additional contribution, originating from the local field inhomogeneities, to the effective transversal relaxation rate R_2^*. Further, $R_2' \approx \gamma \Delta B$ with ΔB representing the field variation and γ the gyromagnetic ratio.

B. Theory: Computersimulation

The aim of the current simulation is to investigate effects on the induced line broadening of the resonance spectra evoked through micro cracks as examples of trabecular rarefaction. Thus, the evaluation of the magnetic field distribution was performed utilizing a two-compartment model, consisting of marrow and bone. In oder to mimic the known trabecular micro structure within a vertebra [13] prolate ellipsoids were arranged appropriately within a three-dimensional unit cell.

The precession frequency of spins in a homogeneous magnetic field is determined through the magnetic induction $\mathbf{B}$. Hence, in a first step the reaction fields induced by the susceptibility difference between the ellipsoids (trabeculae) and the background (bone marrow) were computed [14].

Introducing a sample with a different susceptibility, in the current experiment trabecular bone (χ_2) is surrounded by bone marrow (χ_1), the resulting magnetic induction B_z can be generally written as:

$$B_z = \mu \left(H_{0z} + M_z \left(\mathbf{r} \right) \right) = \mu_0 (1 + \chi) \left(H_{0z} + M_z \left(\mathbf{r} \right) \right), \quad (31)$$

with M_z characterising the induced reaction field. Herin the units are given in the MKS-system, and susceptibility units are per unit volume.

Since the transversal magnetization decay of mineralized bone is several magnitudes faster comparing to bone marrow, the received resonance signal in MR-Osteodensitometry is governed by the magnetization arising within the marrow. Thus M_z corresponds to the computed reaction fields $\Delta H_{r1,z}$ caused by the difference in magnetic property between bone and marrow.

The resulting magnetic field distribution within the unit cell was determined as the sum of the individual contributions H_{zi} originating from all ellipsoids n:

$$\Delta H_{r1,z} \left(\mathbf{r} \right) = \sum_{i=1}^{n} H_{zi} \left(\mathbf{r} \right). \quad (32)$$

Interactions between the trabeculae have been neglected. This assumption is valid, since interactions between such structures include susceptibility effects of the second order, which will give rise to field contributions of the order of $\mathbf{H}_0 \left(\Delta \chi \right)^2$, or $\approx \mathbf{H}_0 \cdot 10^{-12}$.

In a simple MR experiment, excitation followed by an acquisition period, the signal of the free induction decay (FID) can be written as:

$$S(t) = \text{const} \int_{VOI} d^3\mathbf{r} \ e^{-i\omega(\mathbf{r})t} \ e^{-T_2/t}; \quad (33)$$

with $\omega(\mathbf{r}) = \gamma B_z(\mathbf{r})$ it follows:

$$S(t) = \text{const} \int_{VOI} d^3\mathbf{r} \ e^{-i\gamma B_z(\mathbf{r})t} \ e^{-T_2/t}. \quad (34)$$

Using again expression (31) the following expression in $\Delta H_{r1,z}$ can be found:

$$S(t) = \text{const} \int_{VOI} d^3\mathbf{r} \ e^{-i\gamma t \mu_0 (1+\chi)(H_{0z} + \Delta H_{r1,z}(\mathbf{r}))} \ e^{-T_2/t}. \quad (35)$$

This integral must be extended over the entire unit cell enclosing the ellipsoids.

In order to compare the simulation results with MR images the magnitude of $S(t)$ must be found. Except for the dissipative relaxation phenomenon $e^{-T_2/t}$ the expressions in (35) are

purely oscillatory in H_{0z}. Hence, for the analysis of the signal course the essential decay can be expressed as:

$$|S(t)| = \text{const} \int_{VOI} d^3\mathbf{r} \ e^{-i\gamma t \mu_0 (1+\chi)\Delta H_{r1,z}(\mathbf{r})}. \quad (36)$$

$\Delta H_{r1,z}(\mathbf{r})$ can be computed according to (32) as the sum over all the reactions fields of the individual ellipsoids, where $\mu_0(1+\chi)$ describes the magnetic permeability at the location $\mathbf{r}$.

1) Algorithm: Utilizing the expression developed for the reaction field (28) the simulation was implemented in *Mathematica* (Wolfram Research, Inc.). The program computed the field distribution of $\Delta H_{r1,z}(\mathbf{r})$ in the sense of a histogram and generated the MR signal curve according to (36).

As input parameters the spacing of the trabeculae in x-, y- and z-direction, the dimensions of the ellipsoids and the position of the symmetry axis with respect to the z-axis of the coordinate system had to be defined. Further, the susceptibilities of the bones and the background as well as the orientation of the applied homogenous main magnetic field had to be set. The results of the simulations were the histograms of the magnetic field distribution and the signal curve, which was further utilized within a fitting-procedure yielding the relaxation constant R_2'.

2) Data fitting: Utilizing the simulated signal curves a exponential signal model was applied in order to approximate the relaxation time T_2' [15]. The computed signal intensities (36) at the echo times ranging from 0 to 50 ms, 5 ms increment, were used to generate a single T_2' value by means of a non linear least-squares-approximation to a two parameter fit function:

$$S(t) = A \ e^{-t/T_2'} . \quad (37)$$

C. Model of vertebra

The three-dimensional unit cell was composed out of thirty prolate ellipsoids, fifteen aligned along the x- and z-direction each, mimicking the initial intact trabeculae. The interruptions were simulated in the way, that each trabecula was replaced by two ellipsoids, which were displaced along the x/z-axis by 50 μm forming a crack. The configuration of the three-dimensional vertebra model and the applied parameter setting are given in Fig.1.

Intact trabecular network   Network in case of microfractions
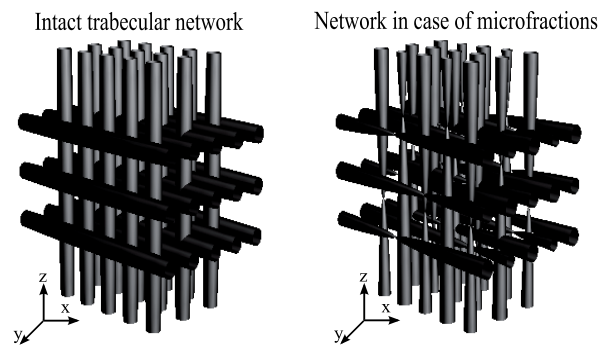

Fig. 1.   Depiction of the $3.75 \times 3.75 \times 3.75 \ mm^3$ unit cell; the x/z aligned sets are built up of three planes displaced by 750 μm. The trabeculae in each plane were modelled with a trabecular spacing and width of 500 μm and 120 μm respectively. The trabecular micro fractures were simulated by replacing each of the intact trabeculae with two opposed shifted versions.

D. Results

The resulting reaction fields H_{r1} pre- and post bone rarefaction are depicted in Fig.2. Note, that the field distribution is directly affected by the shape of the micro cracks, whereby the resulting field inhomogeneities in the vicinity of the spiky edges lead to the observed major field broadening. Prior rarefaction, the inital field distribution ranged approximately around ± 1 A/m, afterwards field values from almost ± 2 A/m were found within the three-dimensional vertebra model. The effect of the interrupted bone mesh on the MR signal decay and the resulting estimated relaxation time T_2' is presented in Fig.3. The modelled cracks gave rise to a change of the initial T_2' of 26.1 ms to approximately 14.4 ms.
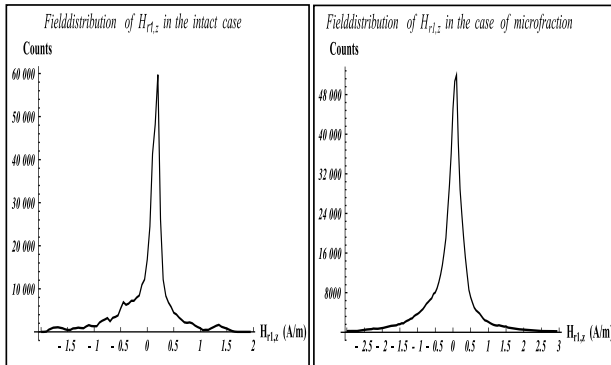

Fig. 2.   Resulting field distribution of the reaction field $H_{r1,z}$ within the applied three-dimensional vertebra model. The trabecular cracks causing a broadening of the distribution, resulting in a more Lorentzian like line shape. A main magnetic field $\mathbf{H}_0 = 2.38732 \cdot 10^6$ A/m with $\alpha = 30°$ and β parallel z-axes, and values of $\chi_1 = -0.62 \cdot 4 \cdot \pi \cdot 10^{-6}$ and $\chi_2 = -0.9 \cdot 4 \cdot \pi \cdot 10^{-6}$ were applied.

V. CONCLUSION

The advantage of this new approach is that it is very easy to build and investigate structures built from spheroids with different axes and positions. There is no need of complicated coordinate transformations.

The analytical solutions of the Laplacian potential problem of spheroids in Cartesian coordinates were successfully applied.
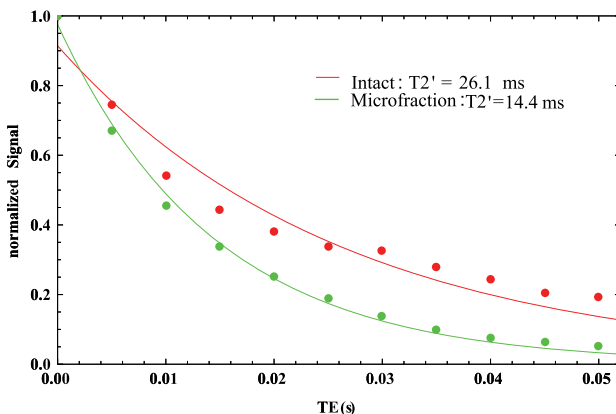

Fig. 3.   Resulting resonance signal decays affected by the reaction field $H_{r1,z}$ of the vertebra model in the two situations. As a consequence of the increasing inhomogeneous reaction field a rapid signal decay in case of micro cracks is visible (green curve). The signals are normalized to the values at the first echo time T_E, markers are indicating the computed signal values at T_E.

A three-dimensional magnetostatic problem in the area of MR-Osteodensitometry, susceptibility effects in the vicinity of micro cracks, was analysed. Within vertebrae affected by pathologies such as osteoporosis horizontally arranged structures get typically interrupted at first. The novel expressions make it possible to study the bone rarefaction along such pathologies, whereby either cracks of the horizontal, the vertical or arbitrary structures are accessible for modelling.

In the present work just one application of the analytical expressions, the modelling of bone disorders in the area of MR-Osteodensitometry, was given. For example in the field of functional MRI the devoloped toolbox eases the analysis of the BOLD (blood oxygenation level-dependent) contrast, where induced reaction fields in the surrounding of vascular networks are of great interest [16]. A fast and precise computation of the magnetic distortion is essential for improving the precision of the temperature determination in techniques using the proton resonance frequency (PRF) shift method [17], [18]. Temperature mapping in the vicinity of the needle electrode is a crucial determinant of MRI guided interventional radiofrequency ablations [19]. Further, in the field of metabolism studies using NMR spectroscopy (MRS) the expressions can be used in order to model specific cells introduced in solutes differing in magnetic susceptibility. [20].

In summary, the authors believe that the novel formulation of solutions depending solely on the Cartesian coordinates will facilitate the modelling of countless magnetostatic problems.

REFERENCES

[1] P. Moon and D.E. Spencer: Field Theory Handbook. Including coordinate systems, differential equations and their solutions. Springer 1988.

[2] P. W. Kuchel, and B. T. Birman, "Perturbation of Homogeneous Magnetic Fields by Isolated Single and Confocal Spheroids. Implications for NMR Spectroscopy of Cells," NMR in Biomedicine, vol.2 (4) pp. 151-160, 1989.

[3] M. Kraiger, and B. Schnizer, "Potential and Field of a Homogeneous Magnetic Spheroid of Arbitrary Direction in a Homogeneous Magnetic Field in Cartesian Coordinates," to appear in COMPEL, 2012.

[4] M. Kraiger, and B. Schnizer, "Reaction Fields of a Homogeneous Magnetic Spheroids of Arbitrary Direction in a Homogeneous Magnetic Field. A Toolbox for MRI and MRS of Heterogeneous Tissue." Report ITPR-2011-021. Institute for Theoretical and Computational Physics. Technische Universität Graz, Austria. http://itp.tugraz.at/~schnizer/MedicalPhysics/

[5] F. W. Wehrli, H. K. Song, P. K. Saha, and A. C. Wright, "Quantitative MRI of the assessment of bone structure and function," NMR in Biomedicine, vol. 19 pp. 731-764, 2006.

[6] C. A. Davis, H. K. Genant, and J. S. Dunham, "The effects of bone on proton NMR relaxation times of surrounding liquids," Investigative Radiology, vol. 21 pp. 472-477, 1986.

[7] S. Grampp, S. Majumdar, M. Jergas, P. Lang, A. Gies, and HK. Genant, "MRI of bone marrow in the distal radius: in vivo precision of effective transverse relaxation times," European Radiology, vol. 5 pp. 43-48, 1995.

[8] T. M. Link, J. C. Lin, D. Newitt, N. Meier, S. Waldt, and S. Majumdar, "Computergestützte Strukturanalyse des trabekulären Knochens in der Osteoporosediagnostik," Der Radiologe, vol. 38 pp. 853-859 , 1998.

[9] M. H. Arokoski, J. P. Arokoski, P. Vainio, L. H. Niemitukia, H. Kroeger, and J. S. Jurvelin, "Comparison of DXA and MRI methods for interpreting femoral neck bone mineral density," Journal of Clinical Densitometry, vol. 5 pp. 289-296. 2002.

[10] H. Chung, F. W. Wehrli, J. L. Williams, and S. D. Kugelmass, "Relationship between NMR transverse relaxation, trabecular bone architecture and strength," Proceedings of the National Academy of Sciences, vol. 90 pp. 10250-10254, 1993.

[11] T. B. Brismar, T. Hindmarsh, and H. Ringertz, "Experimental correlation between T2* and ultimate compressive strength in lumbar porcine vertebrae," Academic Radiology, vol. 4 pp. 426-430, 1997.

[12] O. Beuf, D. C. Newitt, L. Mosekilde, and S. Majumdar, "Trabecular Structure Assessment in Lumbar Vertebrae Specimens Using Quantitative Magnetic Resonance Imaging and Relationship with Mechanical Competence," Journal of Bone and Mineral Research, vol. 16 pp. 1511-1519, 2001.

[13] T. Hildebrand, A. Laib, R. Müller, J. Dequeker, and P. Regsegger, "Direct Three-Dimensional Morphometric Analysis of Human Cancellous Bone: Microstructural Data from Spine, Femur, Iliac Crest, and Calcaneus," Journal of Bone and Mineral Research, vol. 14 pp. 1167-1174, 1999.

[14] C. J. C. Bakker, R. Bhagwandien, M. A. Moerland, and M. Fuderer, "Susceptibility artifacts in 2D FT spin-echo and gradient-echo imaging: the cylinder model revisted," Magnetic Resonance Imaging, vol. 11 pp. 539-548, 1992.

[15] A. Fransson, S. Grampp, and H. Imhof, "Effects of trabecular bone on marrow relaxation in the tibia," Magnetic Resonance Imaging, vol. 17 pp. 69-82, 1998.

[16] S. Ogawa, T. M. Lee, A. R. Kay, and D. W. Tank, "Brain magnetic resonance imaging with contrast dependent on blood oxygenation," Proceedings of the National Academy of Sciences of the United States of America, vol. 87 pp. 9868-9872, 1990.

[17] J. C. Hindman, "Proton resonance shift of water in gas and liquid states," Journal of Chemical Physics, vol. 44 pp. 4582-4592, 1966.

[18] V. Rieke, and K. B. Pauly, "MR Thermometry," Journal of Magnetic Resonance, vol. 27 pp. 376-390, 2008.

[19] A. Boss, H. Graf, B. Müller-Bierl, S. Clasen, D. Schmidt, P. L. Pereira, and F. Schick, "Magnetic susceptibility effects on the accuracy of MR temperature monitoring by the proton resonance frequency method," Journal of Magnetic Resonance Imaging, vol. 22 pp. 813-820, 2005.

[20] P. W. Kuchel, "Red cell metabolism: studies using NMR spectroscopy," Proceedings of Australian Biochemistry Society, vol. 15 pp. P5-P6, 1983.